Geophys. J. R. astr. Soc. (1980) **60**, 289–300

Research note

The Oblique Seismic Experiment on DSDP Leg 52

R. A. Stephen*, K. E. Louden and
D. H. Matthews *Department of Geodesy and Geophysics, Madingley Rise, Madingley Road, Cambridge CB3 0EZ*

Received 1979 May 17; in original form 1978 November 20

Summary. The Oblique Seismic Experiment (OSE) has been proposed to increase the usefulness of the IPOD crustal borehole as a means of investigating layer 2 of oceanic crust. Specific objectives are: to determine the lateral extent of the structure intersected by the borehole, to analyse the role of cracks in the velocity structure of layer 2, to look for anisotropy which may be caused by large cracks with a preferred orientation and, finally, to measure attenuation in oceanic crust.

The first successful Oblique Seismic Experiment in oceanic crust was carried out in 1977 March in a hole 400 miles north of Puerto Rico. An adequate study of lateral velocity variations was impossible because the hole was not deep enough, the hole was inadequately logged, and the small scale basement topography was not known. In general both *P*- and *S*-wave velocity profiles suggest that the crack density decreases with depth in layer 2. Velocities at the bottom of layer 2 are the same as matrix velocities for basalt, implying that crack density may be negligible at this depth. No convincing evidence for anisotropy in either layer 2 or 3 is found from travel time analysis. The hole was not deep enough to measure attenuation from normal incidence shots and amplitudes were not consistent enough to obtain a measure of attenuation from long range shots.

1 Objectives of the OSE

In an OSE shots which have been generated at the surface from small (< 1 km) to large (> 10 km) ranges are received in a borehole (Fig. 1). In oceanic crust, the direct or 'oblique' ray paths impinge on the receiver at angles from 0° to almost 90°.

The OSE has been proposed to increase the usefulness of IPOD (International Phase of Ocean Drilling) crustal drilling as a means of investigating layer 2 in oceanic crust. The experiment has four objectives:

(i) To determine the lateral extent of the structure intersected by the borehole.
(ii) To analyse the role of cracks in the velocity structure of oceanic crust.

* Now at Woods Hole Oceanographic Institution, Woods Hole, MA 02543, USA.

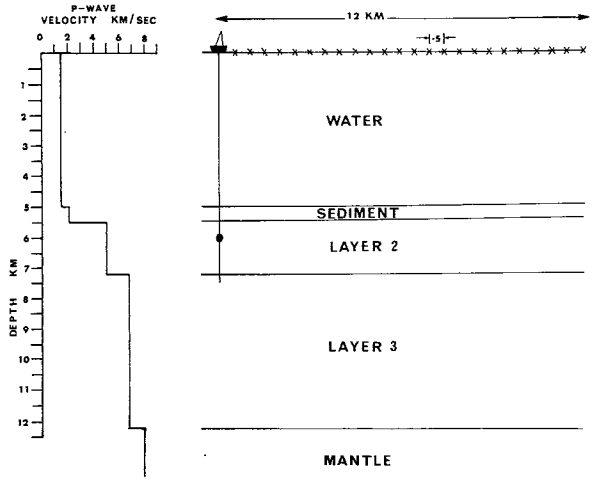

Figure 1. Layout for the OSE over average oceanic crust (Ludwig, Nafe & Drake 1970). The dot represents a receiver depth of 6 km and the crosses indicate the recommended shooting programme for the OSE over oceanic crust.

(iii) To look for anisotropy in layer 2.
(iv) To measure attenuation in oceanic crust.

In the study of layer 2 in oceanic crust the OSE bridges the gap between borehole techniques, such as laboratory analysis of cores and well logging, and conventional seismic refraction which uses sonobuoys, ocean bottom seismometers or ocean bottom hydrophones as receivers. By analysing cores in the laboratory one can study oceanic crust on a scale up to a few centimetres and *in situ* measurements using logging tools can be used to study the oceanic crust up to a few metres from the borehole. However, there is a big difference between these scales and the scale of a marine refraction experiment which is used to look at crust over a few kilometres. The OSE gives information about oceanic crust around the borehole on the scale of hundreds of metres.

2 Operations and data

The first successful OSE in oceanic crust was carried out on Leg 52 of the Deep Sea Drilling Project in Hole 417D (see Fig. 2). The shooting was carried out by the *Virginia Key*, a research vessel from the Atlantic Oceanographic and Meteorological Laboratories of NOAA (National Oceanic and Atmospheric Administration) in Miami. A technical description of the equipment used in the experiment is given by Stephen (1980).

Table 1 summarizes the significant depths in Hole 417D at the time of the experiment. The shooting pattern is shown in Fig. 3. A cross pattern with the *Glomar Challenger* at the centre was fired with the geophone at 6060 m BRF (below rig floor) and a single line from 12 km south-southwest of the drilling vessel to 12 km north-northeast was fired with the geophone at 5840 m BRF. North-northeast is the azimuth of the magnetic lineations in the area. All charges were 20 pounds (~ 9 kg) of Tovex Extra. Shots were fired at approximately 0.5 km intervals on the straight lines and at 2 km intervals on the arcs.

An example of a raw record made during the shooting is shown in Fig. 4. The signal-to-noise ratio of the records is generally good. The majority of the noise is caused by electrical switching on the ship and is the same on all three downhole channels. Since the *P*-wave is stronger on one channel than the other two, the signal-to-noise ratio of first *P*-wave arrivals can be improved by subtracting channels (Stephen, Louden & Matthews, in press).

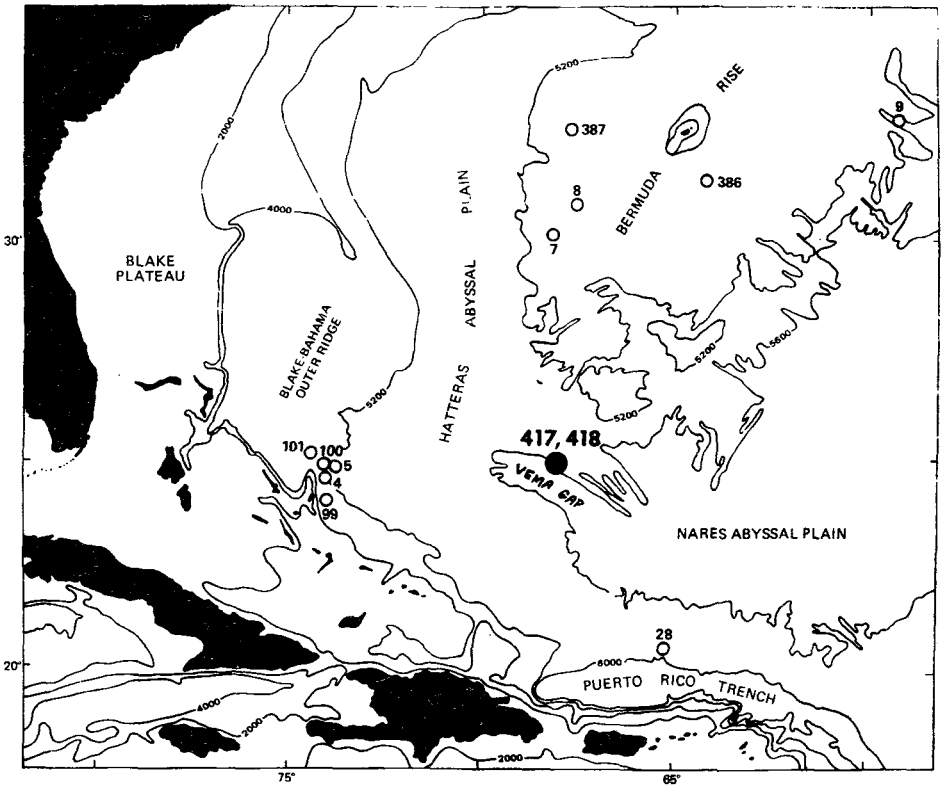

Figure 2. Location of DSDP Sites 417 and 418. (Courtesy of Deep Sea Drilling Project.)

Table 1. Significant depths in Hole 417D.

	Depth from rig floor (m)	Depth from mud line (m)	Depth into basement (m)
Sea level	10		
Mud line	5489		
Casing shoe	5515	26	
Sonic long-top	5637	148	
Basement	5832	343	
Geophone position 2	5840	351	8
Sonic long-bottom	5936	447	104
Leg 51 penetration	6022	533	190
Geophone position 1	6060	571	228
Depth to top of pipe	6092	603	260
Leg 52 penetration	6198	709	366

The total estimated maximum random error in travel-times is ± 0.025 s. Half of this is associated with the flight time correction which could be eliminated if airguns or electrically fired charges were used. Absolute travel-times which are affected by systematic errors as well as random errors were not used in the interpretation.

Regrettably, the *Virginia Key* did not have operating bathymetry or seismic profiling gear so that bathymetry and basement topography were not obtained during the experiment. Seismic profiling had been performed in the area earlier by the *Glomar Challenger* and the

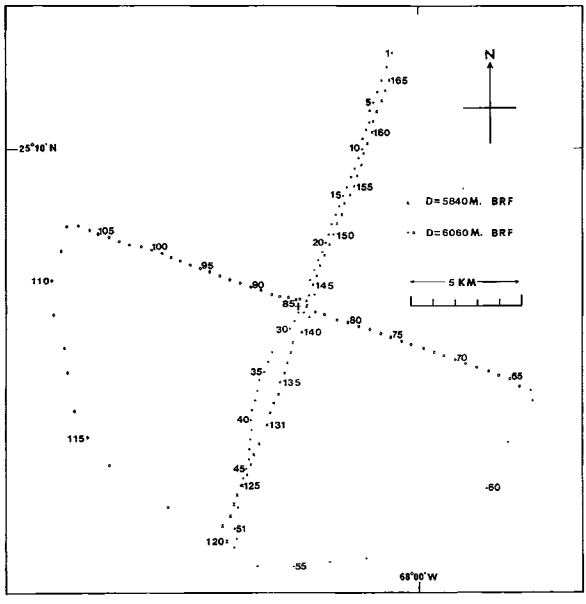

Figure 3. Shot locations relative to the *Glomar Challenger* (+). Ranges were computed from the direct water wave travel-time and bearings were monitored from the *Glomar Challenger* during the experiment. The lines referred to in the text are defined as follows: north (6060 m), shots 1–24; south (6060 m), shots 29–53; east (6060 m), shots 64–84; west (6060 m), shots 87–108; north (5840 m), shots 144–165; south (5840 m), shots 120–141; south-east azimuths, shots 53–63; south-west azimuths, shots 108–119. Lines were shot parallel (NNE and SSW) and perpendicular (ESE and WNW) to the magnetic lineations in the area.

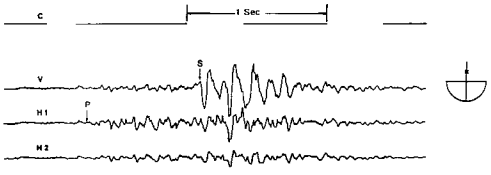

Figure 4. Typical seismogram from a north line. Clock channel (c), vertical component signal (V) and the two horizontal component signals (H1 and H2) are shown as they were recorded on board *Glomar Challenger*. The strongest *P*-wave signal is arriving on the H1 component which implies that the axis of this geophone is aligned approximately N–S. The angle of incidence of the arrivals is large, confirming that at long ranges the direct arrivals are travelling almost horizontally. These seismograms are for a range of 6.58 km and a geophone depth of 6060 m.

USNS *Lynch* (Rabinowitz, Hoskins & Asquith, in press). These lines were used for the bathymetry and basement topography corrections. Unfortunately detailed basement topography (about 200 m high and about 1 km long) could not be resolved from the profiles because of broad diffraction hyperbolae, caused by the geometry in 5500 m of water, and a strong mid-sediment reflector, which masked deeper energy. Errors in travel-times caused by unknown detailed basement topography of ± 200 m are ± 0.085 s for *P*-waves and ± 0.055 s for *S*-waves.

The maximum random error for ranges is ± 29 m for ranges between 0.75 km and 1.00 km. This decreases with range to an error of ± 24 m for ranges greater than 5 km.

A complete set of record sections for all the data collected during the experiment is compiled in Stephen *et al.* (in press).

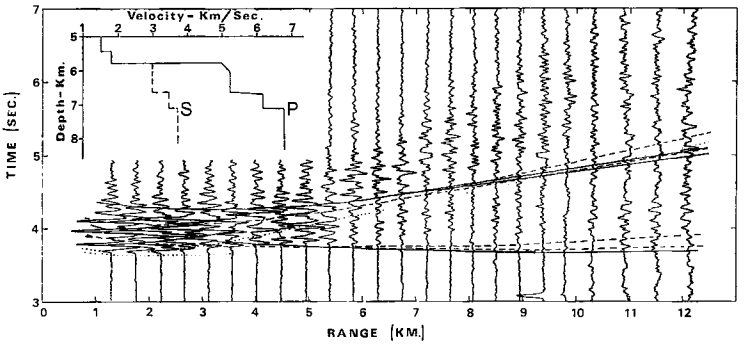

Figure 5. Initial travel-time analysis for the north line with the geophone at its deepest depth. The record section is for the horizontal H1 component. Direct arrivals (....), reflections and refractions from the 6.2 km s^{-1} layer (– – –) and reflections and refractions from the 6.8 km s^{-1} layer (——) are shown for both *P* and *S*-waves. *P*-wave travel-times for arrivals between 7 and 12 km were picked from the difference seismogram constructed by subtracting the vertical and horizontal components (Stephen *et al.*, in press). *S*-wave arrivals are clearer on the vertical component. The reflection curves from the 6.2 and 6.8 km s^{-1} layers were calculated using a ray tracing technique with terrain included. The refracted arrivals are kinked corresponding to the terrain corrections. The seismogram is displayed with a reduction velocity of 6.0 km s^{-1} and an amplitude weighting of $(\text{range}/7.0)^{2.9}$ for ranges greater than 7.0 km.

3 Data interpretation

3.1 INITIAL TRAVEL-TIME INTERPRETATION

A sample record section with an initial travel-time interpretation is shown in Fig. 5. From the direct *P*-wave arrival times (the first arrivals up to 3.5 km range) the *P*-wave velocity in the upper part of layer 2 is estimated at 5.0 ± 0.25 km s^{-1}. (This estimate is refined in the next section.) The first arrivals at ranges between 4.0 and 9.0 km suggest a 6.8 km s^{-1} layer and the 6.2 km s^{-1} layer was introduced to explain the relatively high amplitude arrivals just behind the 6.8 km s^{-1} line at ranges greater than 9.0 km.

The *S*-wave velocities in layer 2 were chosen to give the 3.75 km s^{-1} refraction from layer 3 an acceptable intercept. Depths for the *S*-wave case were taken from the *P*-wave model. Shear waves can be detected better on vertical component seismograms than on horizontal component seismograms because the waves which are detected by the geophone within the basement travel almost horizontally.

3.2 DETAILED TRAVEL-TIME INTERPRETATION

In order to obtain more accurate velocities to look for azimuthal effects, linear regression by the method of least squares was performed on the mid-range *P*-wave refractions, the *S*-wave refraction curve and the direct *S*-wave arrivals. The results of this study are summarized in Table 2. There is no significant evidence for azimuthally dependent velocity in either *P*- or *S*-waves for layer 3 or in *S*-waves for layer 2. The best estimate for layer 3 compressional and shear wave velocities is highest in the north, lowest in the west and about the same in the east and south.

The layer 3 *P*- and *S*-wave refractions give velocities which agree well with the initial model (6.67 ± 0.34 and 3.71 ± 0.10 km s^{-1} compared with 6.8 and 3.75 km s^{-1}). The direct *S*-wave velocity is lower (2.60 ± 0.06 km s^{-1} compared with 3.0 km s^{-1}) but this may be a consequence of an *S*-wave gradient in layer 2. The 2.60 km s^{-1} value was determined from rays which only travelled in upper layer 2 (the top 300 m) but the 3.0 km s^{-1} value

Table 2. Linear regression summary for the six lines. The number in brackets is the number of points used in the velocity determination. The quoted errors are standard deviations.

Line	Layer 3 *P*-velocity (refracted) (km s^{-1})	Layer 3 *S*-velocity (refracted) (km s^{-1})	Layer 2 *S*-velocity (direct) (km s^{-1})
North – D = 6060 m	6.97 ± 0.44 (6)	3.75 ± 0.12 (11)	2.49 ± 0.02 (5)
North – D = 5840 m	6.66 ± 0.20 (7)	3.88 ± 0.02 (6)	2.48 ± 0.04 (6)
South – D = 6060 m	6.70 ± 0.30 (11)	3.63 ± 0.08 (8)	2.61 ± 0.05 (4)
South – D = 5840 m	6.50 ± 0.27 (7)	3.81 ± 0.19 (5)	2.67 ± 0.04 (3)
East – D = 6060 m	6.75 ± 0.44 (8)	3.68 ± 0.11 (6)	2.72 ± 0.21 (4)
West – D = 6060 m	6.46 ± 0.37 (8)	3.51 ± 0.06 (7)	2.60 ± 0.01 (4)
Means	6.67 ± 0.34	3.71 ± 0.10	2.60 ± 0.06

represents a mean velocity for the top 0.9 km. The latter velocity was chosen to obtain a reasonable intercept for the layer 3 *S*-wave refraction.

The upper layer 2 *P*-wave velocity can also be refined. Fig. 6 shows travel-time residuals between the observed data and data for a model with regional topography and a layer 2 *P*-wave velocity of 4.8 km s^{-1}. It appears that detailed basement topography, not resolvable on the reflection profiles, is affecting the travel-times. The 4.8 km s^{-1} velocity was selected because it gave the smallest time discrepancies between deep and shallow geophone positions for the north and south lines. The residuals for the last line show the effect of the hill which was drilled in Hole 417A. The detailed topography appears much less rugged parallel to the magnetic lineations than perpendicular to them, reminiscent of mid-Atlantic ridge topography (Ballard *et al.* 1975; Ballard & van Andel 1977; Macdonald & Luyendyk 1977).

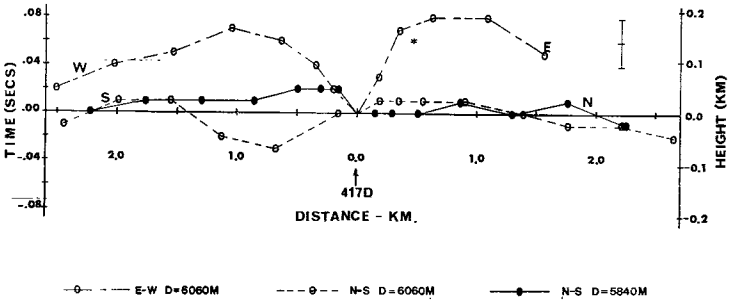

Figure 6. Travel-time residuals between observed travel-times and times calculated assuming a layer 2 velocity of 4.8 km s^{-1} and regional topography. These residuals can be explained by small scale basement topography not seen on the profiling records. Basement terrain is much rougher perpendicular to the spreading axis (E–W) than parallel to it (N–S). The error bars in the upper right hand corner represent 0.025 s which is the estimated timing error in travel times. The smoothness of the curves indicates that the actual error may be somewhat less than this. The star (*) shows the depth of basement at Hole 417A. The deviation in the south lines up to 1.5 km may be the result of the navigation (Fig. 3). All lines pass through the origin by definition. D is the depth of the receiver below rig floor.

There is no point in studying lateral velocity effects from direct arrivals unless the small scale topography is known accurately from detailed profiling. Since sharp features on the sea-bed are masked by diffractions (Laughton, Hill & Allan 1960; Laughton 1963; Speiss & Mudie 1970) conventional reflection profiling may not be adequate in the deep ocean.

3.3 AMPLITUDE ANALYSIS AND SYNTHETIC SEISMOGRAMS

Synthetic seismogram analysis is particularly helpful in studying seismograms which contain a large amount of interference information as in this experiment (Fig. 5). Rather than trying to match the exact amplitudes of an isolated pure phase, it is necessary to consider regions on the seismic section which seem to display characteristic behaviour. The synthetic seismograms here were computed by the reflectivity method as modified by Stephen (1977).

Fig. 7 shows a sample horizontal component seismogram (a) with synthetic seismograms for two models (b, c). Five regions have been circled on the seismograms which exhibit characteristic behaviour. Regions A and B are the critical regions for *P*- and *S*-wave arrivals from layer 3 respectively. Amplitudes in these regions are large when compared to the amplitudes on the section in general. Regions C and D are areas of destructive interference in the *S*- and *P*-wave energy respectively. The observed section shows relatively low amplitudes in these regions. Region E includes the long range layer 3 refraction arrivals and is also an area of low amplitudes.

Fig. 7(b) shows the synthetic seismogram corresponding to the model in Fig. 5. The *P*- and *S*-wave amplitudes in the critical regions (region A and B respectively) are too weak. The *P*- and *S*-wave amplitudes in the interference regions (regions D and C respectively) are too strong and the critically refracted *P*-wave does not die away after 9.0 km (Region E).

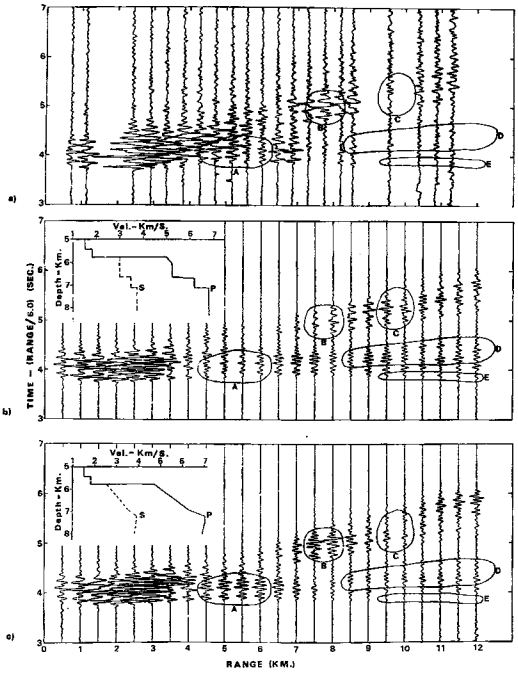

Figure 7. Interpretation of a horizontal component record section for the south line fired to the deep geophone position. Fig. 7(a) is the observed data and Figs (b) and (c) are two synthetic seismograms for the different models shown. The regions A, B, C, D and E are described in the text. All the seismograms shown are displayed with an amplitude weighting of $(\text{range}/7.0)^{2.9}$ for ranges greater than 7.0 km.

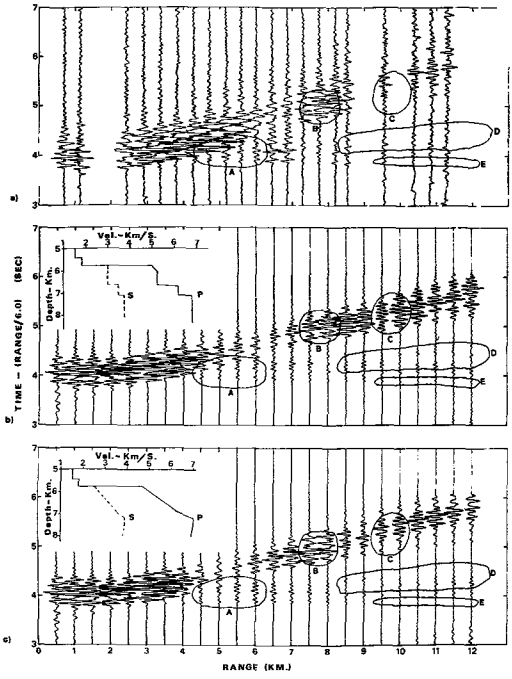

Figure 8. The same as Fig. 7 for the vertical component record section.

The model of Fig. 7(c) produces an acceptable fit to the amplitudes of the observed record section. (Both models fit the travel-time criteria for the observed data.) The interference regions D and C are the most diagnostic regions on the seismograms. The amplitude behaviour in these regions is sensitive to the nature of the boundary between layers 2 and 3 and to the nature of the gradients in layer 2. To obtain acceptable amplitude behaviour in the critical regions A and B, it is only necessary to eliminate constant velocity sections in upper layer 2. Low layer 3 refraction amplitudes at large ranges (region E) can be most easily modelled by putting a low velocity zone in layer 3. A velocity inversion in layer 3 has also been suggested by Salisbury & Christensen (1978).

An amplitude analysis of the corresponding vertical component data is shown in Fig. 8. The same regions have been marked on the sections. In this seismogram, the amplitudes in the early part of region A are lower, and the amplitudes in the latter part of region C are higher than for the horizontal component. Again the gradient model fits the amplitude patterns better than the step model.

The gradient model of Figs 7(c) and 8(c) is preferred. The step model is definitely not acceptable. The preference for gradients rather than steps concurs with work of White (1979), Whitmarsh (1978) and Kennett & Orcutt (1976). The higher velocities at the bottom of layer 2 are consistent with Houtz & Ewing's (1976) results.

An attempt to make any more than a general analysis of the seismograms would be unwise. Comparison of seismograms for all the lines shows significant variation in amplitude patterns within ranges of a kilometre (Fig. 9). The effects of unknown basement topography, lateral variations (possibly in the mid-sediment reflector) and inhomogeneities may be too complex to model adequately by conventional means. Interference effects at ranges where more than one ray path arrive at the same time (e.g. regions C and D) have

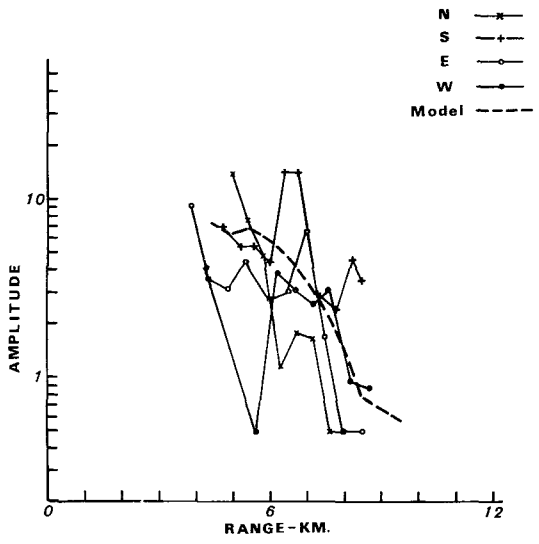

Figure 9. Amplitude–distance curves for the lines fired at the deep geophone position (solid lines) and for the synthetic seismogram of Figs 7(b) and 8(b) (dashed curve). Amplitudes are the root-mean-square peak-to-peak amplitudes of all three components (two components for the synthetic seismograms). These amplitudes correspond to refracted *P*-wave arrivals from layer 3. General trends have been modelled adequately but the observed amplitude data is not consistent or smooth enough to consider more detailed structures or attenuation.

particularly sensitive amplitudes. The use of synthetic seismograms is essential to study these regions.

4 Conclusions

4.1 LATERAL VELOCITY VARIATIONS

The first objective of the OSE was to look for lateral velocity variations in layer 2. This was to be accomplished by determining how far the structure intersected by the borehole extended laterally from the hole.

In the OSE of 1977 March, the hole was only open 260 m into basement and the sonic log was only run for 104 m of this. Consequently, the first requirement for a lateral velocity variation study (i.e. that the seismic structure immediately around the hole is known from sonic logging) was not met. Even if the sonic log had been run as deep as possible, only about 20 per cent of layer 2 would have been logged. (Layer 2 in the area was 1.34 km thick.) The first objective was not accomplished because the drilling was not as successful as anticipated.

In addition, there is little point in looking for lateral velocity variations in layer 2 by travel-time analysis unless the basement topography is known in detail. In the area surrounding Site 417, the profiling was inadequate because of the deep water which spoiled resolution and because of the strong mid-sediment reflector which masked deeper energy. These factors are also mentioned in Houtz & Ewing (1976). Certainly in deep water (> 5.0 km) an improved technique for seismic profiling is required before any seismic technique will be useful in studying detailed lateral velocity variations. The masking effect of the diffraction hyperbolae can be reduced by locating the receivers in the profiling system closer to the sea-bottom. A deep tow system which tows a low frequency sound source and a hydrophone array just above the sea bed would be ideal.

4.2 PORES AND CRACKS

The fact that cracks reduce velocities in some way proportional to their densities is undisputed. The single gradient model of Figs 7(c) and 8(c) satisfies the OSE data adequately. The *P*-velocities increase from 4.8 to 6.4 km s^{-1} with depth in layer 2. Since the extrapolated velocity for zero porosity basalt from laboratory measurements is 6.26 ± 0.10 km s^{-1} (Hamano, in press) it would appear that the effect of cracks diminishes in layer 2 (assuming that layer 2 is the same material throughout), until by the bottom of layer 2 very few cracks are present. Whitmarsh (1978) studied the same effect.

The shear wave velocities from the OSE study behave similarly to the compressional wave velocities. The estimated shear velocity for zero porosity basalt is 3.4 km s^{-1} and the mean shear velocity for cores at atmospheric pressure is 3.1 ± 0.2 km s^{-1} (Hamano, in press). The *in situ* velocities increase from 2.60 to 3.60 km s^{-1} with depth in layer 2.

The confining pressure in layer 3 is generally less than 0.5 kbar (Hyndman 1977) and is insufficient to close the cracks. Evidence for high velocities in lower layer 2 near the mid-Atlantic Ridge (younger than 50 Myr) is inconclusive (Houtz & Ewing 1976). That high crack densities are present near the ridge is implied by the high level of hydrothermal circulation needed to explain the heat flow results (Lister 1972). The scale of these cracks is not known. Why does the crack density decrease with depth? Either hydrothermal or low temperature secondary mineralization seems the most likely answer but why would the cracks start filling at the bottom? An analysis of the process of secondary mineralization with respect to the typical temperature gradients in oceanic crust is required. A comparison of the densities of the three scales of cracks from laboratory (crack dimensions on the order of 5 m), sonic (on the order of 250 cm) and OSE measurements (on the order of 100 m) has been made by Salisbury *et al.* (in press).

4.3 ANISOTROPY

The oriented, linear block faulting observed at the Mid-Atlantic Ridge in the FAMOUS (French American Mid-Ocean Undersea Study) area (by deep sea submersibles (Bellaiche *et al.* 1974; ARCYANA 1975; Ballard *et al.* 1975; Ballard & van Andel 1977) and by deep tow instrument packages (Laughton & Rusby 1975; Macdonald & Luyendyk 1977; Luyendyk & Macdonald 1977) gives a preferred fissure orientation which is the most likely source of upper layer 2 anisotropy. The standard deviation of crack orientation at one site in the inner floor studied by Macdonald & Luyendyk (1977) was only 6°. As the crust moves outward, it is uplifted in a series of normal faults to the rift mountains which again are remarkably well oriented.

No undisputed evidence for preferred crack orientation was found from either velocity or amplitude studies. Rugged basement topography introduces errors into the *P*-wave traveltimes on the order of ± 0.08 s which make accurate velocity determinations over short ranges impossible.

4.4 ATTENUATION

For marine crustal work, both *P*- and *S*-wave attenuation in sediments have been measured (Hamilton 1972, 1976a, 1976b). A measure of attenuation in marine basalts was reported by Neprochnov *et al.* (1967) and Neprochnov (1971) who gave attenuation coefficients from 0.02 to 0.05 (Hamilton 1976a). The OSE is expected to supplement this measure of attenuation in basalts. Because of the shallow hole (260 m into basalt) no determination of attenuation from short range (vertical incidence) shots could be made from the Leg 52 data.

The effects of attenuation on long range shots are much less than the observed amplitude variations which could be caused by undetermined basement topography or lateral inhomogeneities (Fig. 9).

Acknowledgments

The OSE required the assistance and cooperation of a large number of people. We would like to thank Dr J. Heirtzler, Dr H. Stewart, Jr, Dr S. White, Dr W. Bryan, Dr P. Robinson, Mr R. Knapp, Mr V. Larsen, the drilling personnel of *Glomar Challenger* for Leg 52, the DSDP marine technicians, Captain Clarke, the crew of the *Glomar Challenger*, Captain Neill and the crew of the *Virginia Key* for their cooperation in organizing and running the OSE. Dr G. M. Purdy, Mr T. Stetson and Mr J. Broda helped bridge trans-Atlantic communication difficulties and arranged for the explosives. Drs Hoskin and Groman graciously provided the *Lynch* survey data of Site 417. We would like to thank Drs Townsend and Mumford at the Cavendish Laboratory, Cambridge for making their digitizing equipment available and Mr A. Bunch for his digital data reduction programs. We thank Drs B. L. N. Kennett, C. M. R. Fowler, K. Fuchs, G. Müller, V. Červený, I. Pšenčik and Mr D. Wright for making their computer programs available to be modified for the OSE case.

The *Glomar Challenger* ship time was provided by the International Phase of Ocean Drilling and associated organizations. The Natural Environment Research Council funded the other field work and development. The University of Cambridge computing service supplied computer time for the data reduction. We would like to thank Shell Canada Ltd for supporting Stephen's personal expenses for three and a half years.

References

ARCYANA, 1975. Transform fault and rift valley from bathyscaphe and diving saucer, *Science*, **190**, 108–116.

Ballard, R. D., Bryan, W. B., Heirtzler, J. R., Keller, G., Moore, J. G. & van Andel, T. H., 1975. Manned submersible operations in the FAMOUS area: Mid-Atlantic ridge, *Science*, **190**, 103–108.

Ballard, R. D. & van Andel, T. H., 1977. Morphology and tectonics of the inner rift valley at lat. 36° 50′N on the Mid Atlantic ridge, *Bull. geol. Soc. Am.*, **88**, 507–530.

Bellaiche, G., Cheminee, J. L., Francheteau, J., Hekinian, R., LePichon, X., Needham, H. D. & Ballard, R. D., 1974. Inner floor of the rift valley: First submersible study, *Nature*, **250**, 558–560.

Hamano, Y., in press. Physical properties of basalts from Holes 417D and 418D. In *Initial Reports of the Deep Sea Drilling Project*, eds Donnelly, T. W., Francheteau, J., Bryan, W. B., Robertson, P. T., Flower, M. F. J., Salisbury, M. H., *et al.*, volumes 51–53: U.S. Government Printing Office, Washington.

Hamilton, E. L., 1972. Compressional wave attenuation in marine sediments, *Geophysics*, **37**, 620–646.

Hamilton, E. L., 1976a. Sound attenuation as a function of depth in the sea floor, *J. acoust. Soc. Am.*, **59**, 528–535.

Hamilton, E. L., 1976b. Attenuation of shear waves in marine sediments, *J. acoust. Soc. Am.*, **60**, 334–338.

Houtz, R. & Ewing, J. I., 1976. Upper crustal structure as a function of plate age, *J. geophys. Res.*, **81**, 2490–2498.

Hyndman, R. D., 1977. Seismic velocity measurements of basement rocks from DSDP Leg 37. In *Initial Reports of the Deep Sea Drilling Project*, pp. 373–387, eds Aumento, F., Melson, W. G. *et al.*, U.S. Government Printing Office, Washington.

Kennett, B. L. N. & Orcutt, J. A., 1976. A comparison of travel time inversions for marine refraction profiles, *J. geophys. Res.*, **81**, 4061–4070.

Laughton, A. S., 1963. Microtopography. In *The Sea*, Vol. 3, pp. 437–472, ed. Hill, M. N., John Wiley and Sons, New York.

Laughton, A. S., Hill, M. N. & Allan, T. D., 1960. Geophysical investigations of a seamount 150 miles north of Madeira, *Deep Sea Res.*, **7**, 117–141.

Laughton, A. S. & Rusby, J. S., 1975. Long range sonar and photographic studies of the median valley in the FAMOUS area of the Mid-Atlantic Ridge near 37° N, *Deep Sea Res.*, **22**, 279–298.

Lister, C. R. B., 1972. On the thermal balance of a mid-ocean ridge, *Geophys. J. R. astr. Soc.*, **26**, 515–535.

Ludwig, W. J., Nafe, J. E. & Drake, C. L., 1970. Seismic refraction. In *The Sea*, Vol. 4, pt 1, pp. 53–84, ed. Maxwell, A. E., John Wiley and Sons, New York.

Luyendyk, B. P. & Macdonald, K. C., 1977. Physiography and structure of the inner floor of the FAMOUS rift valley: observations with a deep-towed instrument package, *Bull. geol. Soc. Am.*, 88, 648–663.

Macdonald, K. C. & Luyendyk, B. P., 1977. Deep-tow studies of the structure of the Mid-Atlantic Ridge crest near lat. 37° N, *Bull. geol. Soc. Am.*, 88, 621–636.

Neprochnov, Yu.P., 1971. Seismic studies of the crustal structure beneath the seas and oceans, *Oceanology* (English translation), **11**, 709–715.

Neprochnov, Yu.P., Neprochnova, A. F., Zverev, S. M. & Mironova, V. I., 1967. Deep seismic sounding of the earth's crust in the central part of the Black Sea depression. In *Problems in Deep Seismic Sounding*, pp. 44–78, ed. Zverev, S. M., English translation, Consultants Bureau, New York.

Rabinowitz, P., Hoskins, H. & Asquith, S., in press. Geophysical site survey results near DSDP Sites 417 and 418 in the Central Atlantic Ocean. In *Initial Reports of the Deep Sea Drilling Project*, Vol. 51–53, eds Donnelly, T. W., Francheteau, J., Bryan, W. B., Robertson, P. T., Flower, M. F. J., Salisbury, M. H., *et al.*, U.S. Government Printing Office, Washington.

Salisbury, M. H. & Christensen, N. I., 1978. The seismic velocity structure of a traverse through the Bay of Islands Ophiolite Complex, Newfoundland, an exposure of oceanic crust and upper mantle, *J. geophys. Res.*, 83, 805–817.

Salisbury, M. H., Stephen, R. A., Hamano, Y., Johnson, D., Donnelly, M., Francheteau, J. & Christensen, N., in press. The physical state of the upper levels of Cretaceous basement from the results of logging, laboratory studies and the Oblique Seismic Experiment at DSDP Site 417D. In *Initial Reports of the Deep Sea Drilling Project*, Vol. 51–53, eds Donnelly, T. W., Francheteau, J., Bryan, W. B., Robertson, P. T., Flower, M. F. J., Salisbury, M. H., *et al.*, U.S. Government Printing Office, Washington.

Spiess, F. N. & Mudie, J. D., 1970. Small scale topographic and magnetic features. In *The Sea*, Vol. 4, pt 1, pp. 205–259, ed. Maxwell, A. E., John Wiley and Sons, New York.

Stephen, R. A., 1977. Synthetic seismograms for the case of the receiver within the reflectivity zone, *Geophys. J. R. astr. Soc.*, **51**, 169–181.

Stephen, R. A., 1978. The Oblique Seismic Experiment in Oceanic Crust, *PhD thesis*, University of Cambridge.

Stephen, R. A. 1980. The Oblique Seismic Experiment in Oceanic Crust – Equipment and Technique, *Mar. Geophys. Res.*, in press.

Stephen, R. A., Louden, K. E. & Matthews, D. H., in press. The Oblique Seismic Experiment on DSDP Leg 52. In *Initial Reports of the Deep Sea Drilling Project*, Vol. 51–53, eds Donnelly, T. W., Francheteau, J., Bryan, W. B., Robertson, P. T., Flower, M. F. J., Salisbury, M. H., *et al.*, U.S. Government Printing Office, Washington.

White, R. S., 1979. Oceanic upper crustal structure from variable angle seismic reflection–refraction profiles, *Geophys. J. R. astr. Soc.*, 57, 683.

Whitmarsh, R. B., 1978. Seismic refraction studies of the upper igneous crust in the north Atlantic and porosity estimates for layer 2, *Earth Planet. Sci. Lett.*, 37, 451–564.